Optimizing wave energy parks with over 1000 interacting point-absorbers using an approximate analytical method

Malin Göteman[a,*], Jens Engström[a], Mikael Eriksson[a,b], Jan Isberg[a]

[a] *Department of Engineering Sciences, Uppsala University, Sweden*
[b] *Seabased Industry AB, Uppsala, Sweden*

Abstract

Large arrays of wave energy converters of point-absorber type are studied using an approximate analytical model. The model is validated against a numerical method that takes into account full hydrodynamic interactions based on linear potential flow theory. The low computational cost of the analytical model enables parameter studies of parks in the MW range and includes up to over 1000 interacting devices. The model is actuated by irregular wave data obtained at the Swedish west coast. In particular, focus is on comparing park geometries and improving park configurations to minimize the power fluctuations.

Keywords: wave energy parks, hydrodynamics, power fluctuations

1. Introduction

Since the initial works on wave energy [1], research has lead to many different approaches to convert energy in ocean waves to electricity, which has resulted in numerous different techniques. This paper concerns point-absorber wave energy converters (WECs), where a cylindrical buoy at the sea surface is connected to a bottom-mounted linear generator through a line.

To produce power of more than a few MW and enable an even power distribution, future designs will necessarily include arrays of many absorbing units. As the individual units in these wave power parks interact by scattered and radiated waves, the numerical simulations get very heavy when the number of interacting bodies grow. In certain situations, assumptions can simplify the calculations and enable simulations of a large number of structures.

The electricity produced by a point-absorber WEC with linear generator will fluctuate with the incoming waves. In order to connect wave energy parks to the electric grid, means must be taken to reduce the power fluctuations inherent in the wave source. Luckily, the hydrodynamical interactions between WECs in a wave energy park can be used to smoothen out the power fluctuations, a fact that was discussed already in early works on wave energy [2, 3]. With the recent commercialization and full-scale implementation of wave energy, the area has received new attention [4–8]. Although a lot of papers have studied arrays of a few WECs or larger

*Corresponding author

Email addresses: malin.goteman@angstrom.uu.se (Malin Göteman), jens.engstrom@angstrom.uu.se (Jens Engström), mikael.eriksson@seabased.com (Mikael Eriksson), jan.isberg@angstrom.uu.se (Jan Isberg)

arrays in regular waves, so far, there are few publications on full-scale experiments of WEC arrays, and/or large-scale arrays in irregular waves. In [9], experiments with up to three full-scale point-absorber devices were conducted off-shore at the Swedish west coast. It was shown that the standard deviation of power delivered to the electrical substation reduces with 30% and 80% with two and three WECs, respectively, as a mean for an arbitrary array member. In a recent paper [10], scale experiments performed in a wave basin with 25 heaving WECs were presented. For long-crested waves, around 17% reduction in significant wave height was observed downwave the WEC array.

The aim of this paper is to study wave energy parks in the MW regime and with over 1000 WECs, with the particular focus on maximizing power absorption while lowering the power fluctuations. In three earlier papers [11–13], properties of wave energy parks were studied as functions of various parameters. In the first two papers, the hydrodynamical interaction between devices was calculated using the boundary element potential flow solver WAMIT. The method is robust and reliable, but the computational cost for large parks is high and each array configuration must be studied separately by trial and error. As an alternative, here an approximate semi-analytical method is used. Instead of studying each park configuration separately, the parameters can be varied continuously and give hints of optimal configurations. To lower the computational cost and enable simulations of a larger number of interacting structures, here the hydrodynamical interaction due to scattered waves has been neglected, but interactions due to radiated waves is included between all the WECs. Despite this approximation, the model shows good agreement with the standard numerical model for the parks where both methods have been applied.

2. Theory

2.1. Linear potential flow theory

Consider a volume of fluid with finite depth h and define a global coordinate system (x, y, z) such that $z = -h$ at the seabed and $z = 0$ at the undisturbed free sea surface, and N floating cylinders with radius R and draft d, labeled by indices $j \in [1, N]$, and constrained to move in heave only. Divide the fluid domain into interior and exterior domains underneath and outside each buoy. Under the assumption of incompressible, homogeneous fluid density and negligible viscosity and vorticity, the governing equation reduces to the Laplace equation $\Delta\Phi = 0$, where Φ is the fluid velocity potential. Under the assumption of non-steep waves, the non-linear boundary condition at the free sea surface can be linearized and the first order approximation taken. In addition, the fluid is not penetrating the seabed or the floating bodies, and the full linear boundary conditions are

$$\left.\frac{\partial\Phi}{\partial t} + gz\right|_{z\approx 0} = 0, \qquad \left.\frac{\partial\Phi}{\partial z}\right|_{z=-h} = 0, \qquad \left.\frac{\partial\Phi}{\partial n}\right|_{S_B} = V_n, \tag{1}$$

where n is the normal direction of the body surface. For bodies that are not oscillating, the last boundary constraint in (1) is the condition that the fluid should not penetrate the body surface, $\partial_n\Phi| = 0$. Under the assumption that the time-dependence is sinusoidal, it can be factored out as $\Phi(x, y, z, t) = \mathrm{Re}(\phi(x, y, z)e^{-i\omega t})$, where the angular frequency ω is related to the wave number k through the dispersion relation $\omega^2 = gk\tanh(kh)$. In the frequency domain, the first of the boundary conditions in (1), the linearized Bernoulli equation, simplifies to $-\omega^2\phi + g\frac{\partial\phi}{\partial z} = 0$ at the sea surface.

Due to the linearity of the problem, the fluid potential will be a linear superposition of incoming waves, scattered waves among the fixed cylinders, and radiated waves from the bodies own oscillations, $\phi = \phi_{\mathrm{in}} + \phi_S + \phi_R$.

2.2. Solving the diffraction and radiation problems

A general solution to the Laplace equation and the boundary conditions in the exterior domain can be found by separation of variables. In local cylindrical coordinates (r, θ, z) with origin in the center of cylinder j, the solution takes the form

$$\phi^{\text{ext},j} = \sum_{n=-\infty}^{\infty} \left[\sum_{m=0}^{\infty} Z_m(z) \left(A_{mn}^j \frac{K_n(k_m r)}{K_n(k_m R)} + B_{mn}^j \frac{I_n(k_m r)}{I_n(k_m R)} \right) \right] e^{in\theta}, \tag{2}$$

where $Z_m(z)$ are normalized vertical eigenfunctions, $Z_m(z) \propto \cos(k_m(z+h))$. The wave number $k_0 = -ik$ is a root to the dispersion relation above and $K_n(k_0 r) \propto H_n^{(1)}(kr)$ and $I_n(k_0 r) \propto J_n(kr)$ correspond to propagating modes. The wave numbers k_m for $m > 0$ are roots to the dispersion relation $\omega^2 = -gk \tan(kh)$ and correspond to evanescent modes. The unknown coefficients in the potentials will be found by requiring continuity between the exterior and interior regions of each buoy.

2.2.1. Diffraction problem

The diffraction problem is the solution to the scattering among fixed cylinders. Consider a cylinder with center at $(x_j, y_j, 0)$ and an incoming wave with amplitude A, traveling along the x-axis,

$$\phi_{\text{in}}^j = -\frac{iAg}{\omega} \frac{\cosh(k(z+h))}{\cosh(kh)} e^{ikx_j} e^{ikr\cos\theta} = \sum_{n=-\infty}^{\infty} Z_0(z) A_{\text{in},n}^j J_n(kr) e^{in\theta}, \tag{3}$$

where $A_{\text{in},n}^j = -igA/\omega \cdot e^{ikx_j} i^n / Z_0(0)$. The surface elevation of the free surface is $\eta(x, y, t) = Ae^{i(kx-\omega t)}$.

In the general case, the incoming wave on a buoy will be a superposition of ϕ_{in}^j and the scattered waves from the remaining cylinders. The multiple scattering method for determining the fluid velocity potential in an array of floating cylinders was presented in [14]. In the case of bottom-mounted cylinders, the method is completely analytical, whereas for floating bodies, infinite expansions of the eigenfunctions need to be truncated and the method is only semi-analytical. In a *single-body* diffraction problem, used as an approximation in this paper, the contribution from scattered waves of the remaining buoys is neglected, and the diffracted wave in the exterior region of the buoy will be a superposition of the incoming wave (3) and a scattered wave on the form in (2).

Defining $\lambda_n = \pi n/(h-d)$, an ansatz for the diffraction potential in the interior domain underneath the cylinder can be written on the form

$$\phi_D^{\text{int},j} = \sum_{n=-\infty}^{\infty} \left[\gamma_{n0}^j \left(\frac{r}{R} \right)^{|n|} + 2 \sum_{m=1}^{\infty} \gamma_{nm}^j \cos(\lambda_m(z+h)) \frac{I_n(\lambda_m r)}{I_n(\lambda_m R)} \right] e^{in\theta}. \tag{4}$$

Requiring continuity for the diffraction potential between the exterior and interior regions imply that the unknown coefficients γ_{mn} can be found in terms of A_{mn} and B_{mn}. Further requiring continuity for the radial derivative of the diffraction potential again relates the unknown coefficients, and the coefficients can be solved for.

2.2.2. Radiation problem

The radiation potential ϕ_R is the solution to the problem of heaving cylinders and no incoming waves ϕ_{in}. In the interior domain underneath the cylinder, the general solution is given as a sum of a particular and a homogeneous solution,

$$\phi_R^{\text{int},j} = (h-d)V^j \sum_{n=-\infty}^{\infty} \Big[\frac{1}{2(h-d)^2}((z+h)^2 - \frac{r^2}{2}) + a_{0n}(\frac{r}{R})^{|n|} + \sum_{m=1}^{\infty} a_{mn}\cos(\lambda_m(z+h)) \frac{I_n(\lambda_m r)}{I_n(\lambda_m R)} \Big] e^{in\theta}, \quad (5)$$

where $V^j(\omega)$ is the velocity of the buoy in heave and a_{mn} are unknown coefficients. The general solution in the exterior domain is given on the form (2) with only outgoing waves, i.e., $B_{mn} = 0$. Again, requiring continuity between the regions solves for the unknown coefficients and the radiation potential can be determined.

2.3. Dynamical equations

The force of the waves on the floating bodies is given by the pressure integrated along the wetted surface of the cylinder. In the frequency domain, this is proportional to the wave potentials,

$$\bar{F} = i\omega\rho \iint_S [\phi_{\text{in}} + \phi_S] d\bar{S} + i\omega\rho \iint_S \phi_R d\bar{S}. \quad (6)$$

The first term resulting from the incoming and scattered waves, is the excitation force factor f_{exc}; the second term originating from the radiated waves is the radiated force f_{rad}, with real and imaginary parts proportional to the added mass and damping coefficients, respectively. Here, scattering of radiated waves will be neglected, and the interaction by radiated waves, i.e. the non-diagonal terms of f_{rad} will be given by the radiated wave from WEC j when incoming on WEC i, integrated over the wetted surface of WEC i, $f_{\text{rad}}^{ij} = i\omega\rho \iint_{S^i} \phi_R^j|_i dS$. After the diffraction and radiation potentials have been determined as described in section 2.2, the hydrodynamical forces can be readily obtained.

The dynamics of each buoy is determined by Newton's second law $F_{\text{tot}}(t) = m\ddot{z}(t)$, where the total force is a sum of the exciting force F_{exc} from the incoming waves, the damping force from the radiated waves F_{rad}, the statical restoring force for submerged bodies $F_{\text{stat}} = -\rho g\pi R^2 z$ and the power take-off force $F_{\text{PTO}} = -(k_s z + \gamma\dot{z})$. In the frequency domain, the equation of motion can be written in terms of a transfer function

$$H(\omega) = \frac{f_{\text{exc}}(\omega)}{-(m + m_{\text{add}}(\omega))\omega^2 - i(B(\omega) + \gamma)\omega + \rho g\pi R^2 + k_s}, \quad (7)$$

where m is the total mass of the translator and the submerged buoy. After a Fourier transform of the transfer function to the time domain $h(t) = \widehat{H(\omega)}$, the vertical position of the buoy in every time-step is then obtained as a convolution with the incoming wave amplitude, $z(t) = (h * \eta_{\text{in}})(t)$. With the position of the buoy in time determined, the absorbed power of the WEC can be calculated as $P(t) = \gamma\dot{z}(t)^2$.

The performance of a WEC is usually measured in terms of a power capture ratio (PCR) between the time-averaged power absorption and the incident energy transport over the buoy diameter, PCR $= \bar{P}/(2RJ)$, where the incident energy transport for waves in waters of infinite depth can be defined as $J = (\rho g^2/64\pi)T_e H_s^2$.

As described above, one of the most important effects of park interactions is the reduction of power fluctuations. The fluctuations in a park with N WECs can be measured in terms of the normalized variance of the total power, $v = \sigma^2(P_{\text{tot}})/\overline{P_{\text{tot}}}^2$, where σ is the standard deviation and $\overline{P_{\text{tot}}}$ the time-averaged power.

Table 1: The irregular sea states used in the paper, characterized by their energy periods T_e and significant wave heights H_s. The wave data is measured off-shore at the Swedish west coast.

#	T_e[s]	H_s[m]	#	T_e[s]	H_s[m]	#	T_e[s]	H_s[m]	#	T_e[s]	H_s[m]	#	T_e[s]	H_s[m]
1	3.89	0.51	8	4.35	0.80	15	4.86	0.82	22	5.24	1.12	29	6.03	1.06
2	3.95	0.49	9	4.51	0.78	16	4.86	1.14	23	5.29	0.93	30	6.25	2.37
3	4.02	0.72	10	4.51	0.78	17	4.94	1.27	24	5.37	0.93	31	6.54	2.15
4	4.13	0.67	11	4.53	0.79	18	5.01	0.93	25	5.47	1.02	32	6.74	2.52
5	4.21	0.62	12	4.56	0.77	19	5.16	1.39	26	5.60	1.15	33	7.01	1.44
6	4.22	0.78	13	4.68	1.13	20	5.19	1.07	27	5.61	1.13	34	7.30	2.36
7	4.26	0.77	14	4.85	1.31	21	5.21	1.00	28	5.76	1.03	35	5.01	1.53

3. Method

3.1. Model specification

The wave energy converters used in the simulations are of point-absorber type, with a semi-submerged buoy at the sea surface connected to a direct-driven linear generator at the seabed. As such, it resembles the WEC model developed at the Uppsala University, see, e.g., [15–17]. The physical dimensions of the WECs are given by the buoy radius $R = 2$ m, draft $d = 0.5$ m, translator mass $m_t = 2560$ kg, spring constant $k_s = 4$ kN/m, and power take-off damping coefficient $\gamma = 55$ kNs/m. The water depth is $h = 25$ m.

The Uppsala University WECs are deployed at an off-shore research site for full-scale experiments, located on the west coast of Sweden. At this test site, 44% of the annual energy flux occurs for sea states characterized by an energy period T_e in the interval 4-7 s and a significant wave height H_s in the interval 1-3 m [18]. For the simulations, measured time series of the elevation of irregular waves obtained at the test site are used to actuate the buoy and translator. Monodirectional waves propagating along the x-axis are used for all the simulations. The 35 different sea states were obtained at a sampling rate of 2.56 Hz and during time periods of 30 minutes by the commercial Datawell Waverider buoy. The wave data cover the predominant sea state at the research test site at the Swedish west coast and are characterized by the energy period and significant wave high given in table 1. Variations in the water level due to tides and air pressure variations are very small and have been neglected in this paper. In the simulations, the time series were repeated once, so that in total the simulations could model wave energy parks during one hour. To compare performance of different parks, the time averaged power for individual WECs and for the full park have been used. Note that the time averaged power for a WEC differs from and should not be confused with the rated power or the peak power, that are in general much higher than the power obtained as a mean over time.

As explained in section 2, the dynamical parameters in the equations of motion for the buoy are the integrals of the wave potentials in equation (6), i.e. the exciting force, the added mass and the radiation damping. In this paper, we solve for the hydrodynamical coefficients f_{exc}, m_{add} and B using an approximate analytical method. The method is compared with a numerical method using WAMIT, a commercial boundary element potential flow solver. The two methods are discussed in section 3.2. The hydrodynamical coefficients are then used as inputs in a time-domain model in Matlab, where the dynamics of the WECs and the absorbed power are calculated according to the equations in section 2.3.

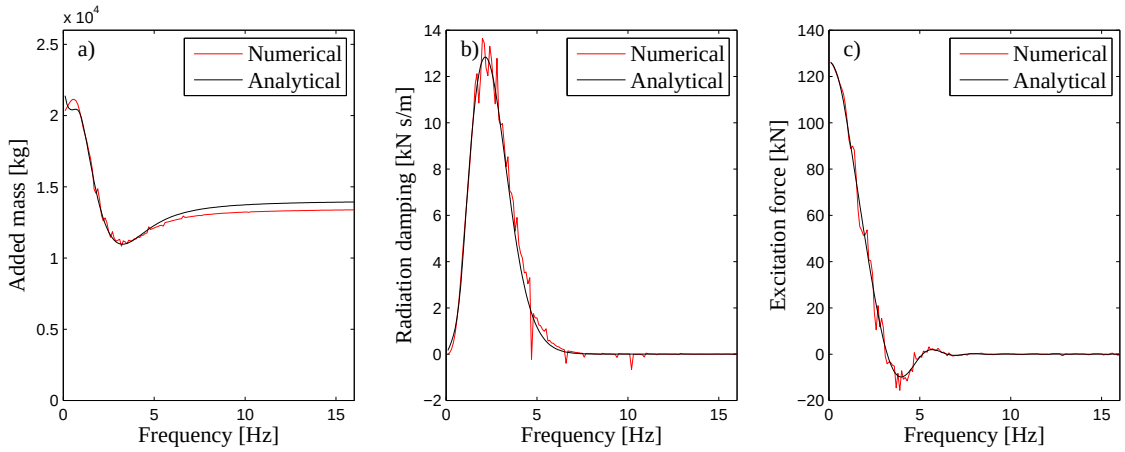

Figure 1: Comparison between the hydrodynamical coefficients calculated by the numerical and the semi-analytical model for a system of four WECs. The plot for the excitation force shows the real part of the excitation force for one of the WECs. The plots for the other WECs show a similar agreement between the numerical and analytical model.

3.2. Numerical and semi-analytical approach

In the numerical approach, the hydrodynamical coefficients in equation (6) are calculated using the commercial boundary element potential flow solver WAMIT.

In the semi-analytical approach, the hydrodynamical parameters are calculated analytically using the method discussed in section 2.2. To obtain numerical values, the infinite expansions in the eigenfunctions must be truncated, hence the method is *semi*-analytical. To achieve 1% accuracy, it is rarely necessary to go beyond 20 equations [19]. Hence, in this paper, the cut-off order has been chosen to $\Lambda = 20$. The hydrodynamical forces are determined by integrating the potentials along the bottom of the cylinders as in equation (6).

The output both from WAMIT and from the semi-analytical method are used to obtain the transfer function (7) in the frequency domain, transform it into the time-domain and compute the dynamics of the individual buoys as a convolution with the incoming wave, as described in section 2.3.

3.3. Approximations and validity of the model

3.3.1. Linear approximation

The linear approximation is valid only for non-steep waves. The irregular waves used to actuate the model are measured outside the Swedish west coast, where the wave climate in general is relatively moderate. The sea states used in the simulations are listed in table 1 and have significant wave heights in the range $H_s \in [0.49, 2.52]$ m. In [20], the WEC model based on the numerical calculation of the hydrodynamical forces was validated with full-scale experiments off-shore at the same location where the used wave data has been obtained.

3.3.2. WEC approximations

The WEC model is assumed to have stiff line between the buoy and the translator, linear power take-off force and heave motion only, i.e. the buoys are constrained to move only vertically. In particular the last assumption of heave motion is crude, in particular for WECs deployed

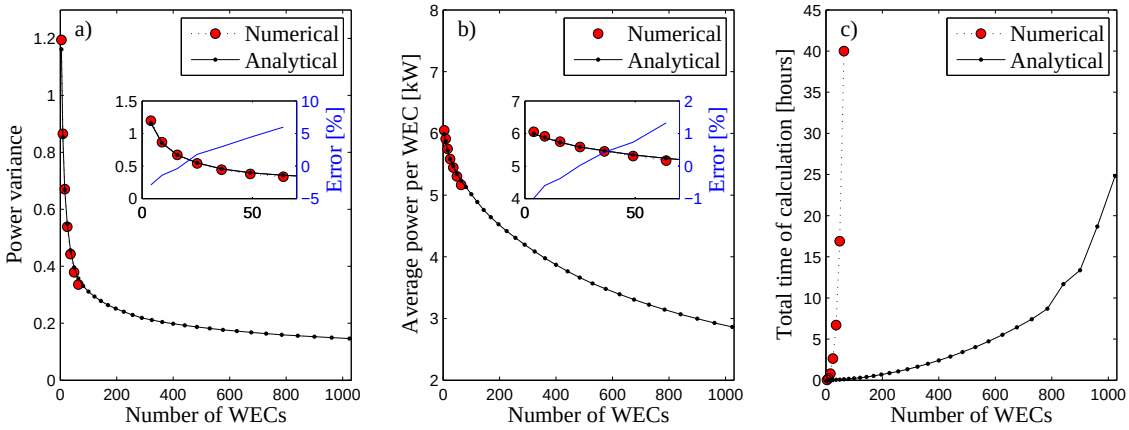

Figure 2: Comparison between the numerical standard method and the approximate semi-analytical method. Power and power variance are calculated for square parks with 2×2 up to 32×32 WECs. The sea state is characterized by energy period $T_e = 5.01$ s and significant wave height $H_s = 1.53$ m. A zoom for number of WECs ≤ 64 is provided in each plot; the blue line shows the deviation of the approximative analytical from the numerical method. The agreement between the models is rather good but seems to grow with increasing number of WECs. The rightmost plot shows that the computational cost of the approximate analytical method is much lower than that of the numerical method, due to the fact that multiple scattering is neglected.

in shallow waters. Despite these assumptions, the numerical WEC model has been validated with good agreement with full-scale experiments off-shore [20]. However, one should bear in mind that the model represents a simplification of the physical system. If one is interested to study more realistic systems including, for example, non-linear physical events such as snap-loads in the line, the assumptions are not valid and a more general model must be used.

3.3.3. Approximations on hydrodynamical interaction

Regarding the hydrodynamical interactions between the buoys, the point-absorber approximation [21–23] has been made in the semi-analytical method, i.e., the buoys are assumed to be so small that their scattered waves do not interact with the remaining buoys. This means that interactions between the buoys is due to their non-scattered radiated waves, and only single-body diffraction is considered for the excitation force. The point-absorber assumption has been found to be a good approximation for large separating distances $D > 8R$, in particular for low frequencies $kR < 0.8$ [24, 25]. The error is expected to grow with increased number of interacting structures, however. On the other hand, the larger number of structures increase the run time of the simulations and prevent calculations of the full interactions between all devices.

In the numerical method full hydrodynamical interactions are included. Hence, the numerical method can be used to verify the approximate analytical method. In figure 1, the added mass, radiation damping and excitation force have been calculated using the numerical and the analytical model in a system of four heaving buoys on a distance $D = 20$ m from each other. For high frequencies, the added mass computed by the approximate method deviates slightly from the one computed by the numerical method. A better agreement would be obtained for a higher cut-off order Λ, but the impact on the results for computed power and power variance in the park would be small. The small fluctuations in the results from the numerical method are due to interaction by scattered waves. Whereas these small fluctuations are not captured by the approximate

analytical method, the overall agreement is good.

In figure 2, the average power per WEC and the power fluctuations, measured in terms of the normalized variance, have been calculated by the full numerical and the approximate analytical methods. The third plot shows the time needed for the simulations. Both simulations have been performed on a standard desktop PC with Intel(R) Xeon(R) 3.07 GHz processor and 6 MB RAM. The wave energy parks studied are all square parks with increasing number of devices, from 2×2 WECs up to 32×32 WECs. The separating distance between all adjacent devices is $D = 20$ m. The numerical method that accounts for full multiple scattering is able to simulate parks with up to $8 \times 8 = 64$ WECs before the computational costs get out of hand. For parks up to this size, the agreement with the approximate analytical method is rather good; however, for large parks the approximate analytical model seems to over-predict both the power variance and average power per WEC slightly. The relative error for a park with 64 WECs is just below 6% for the power variance and less than 1.5% for the average power per WEC. Due to the computational limits of the numerical method, the relative error for larger parks cannot be determined, but is expected to grow with number of WECs. Also, in figure 6a, the power variance has been calculated in both methods as a function of the separating distance between adjacent devices, and the agreement between both methods is good.

The agreement between the models justifies the use of the approximate method also for larger parks, where the numerical method becomes too heavy, but the analytical method readily enables simulations of parks with over 1000 WECs. However, caution should be taken when evaluating the results for very large parks and for parks with WECs in close proximity, since experimental validation of the model has not yet been performed, and since agreement between the two models has only been verified for parks up to medium size.

4. Results

4.1. Comparison of global geometries

Four global geometries with approximately the same number of WECs have been compared in figure 3: the wedge and rectangular shapes have 252 WECs each, whereas the circular and random geometries have 256 WECs each. More specifically, the wedge configuration consists of 4×7 wedges, each with 9 WECs in a single row. The rectangular geometry has 12×21 WECs and the circular geometry contains 8 semi-circles, each with 32 WECs in a double shell. In the wedge and the circle geometries, the separating distance between adjacent WECs is 20-30 m. In the rectangular geometry, the separating distance is 55 m and in the random geometry, the devices are never closer than 6 m from each other. The total used ocean area is comparable for all four configurations. In the figure, the positions of the WECs in the park as well as the time-averaged power per WEC is plotted. For all the geometries, WECs far away from the incoming wave absorb less power. However, as seen in the rectangular configuration, it is not necessarily the WECs in the first row that absorbs most energy; rather it is the third row, showing the positive interference effect of the radiated waves from the other buoys in the park. For reference, an isolated WEC in the same wave climate as in figure 3 would have an absorbed power of 2.4 kW. Some of the WECs in figure 4 have a time-averaged power absorption of 2.7 kW, which is 13% more than the absorbed power in isolation. As has been discussed in [8], the fact that radiated waves from WECs far away from the incident wave are affecting the WECs in the front rows is a unique feature of wave energy parks as compared to, for example, wind energy farms, where a wake is induced behind every device and the front row is expected to absorb most energy.

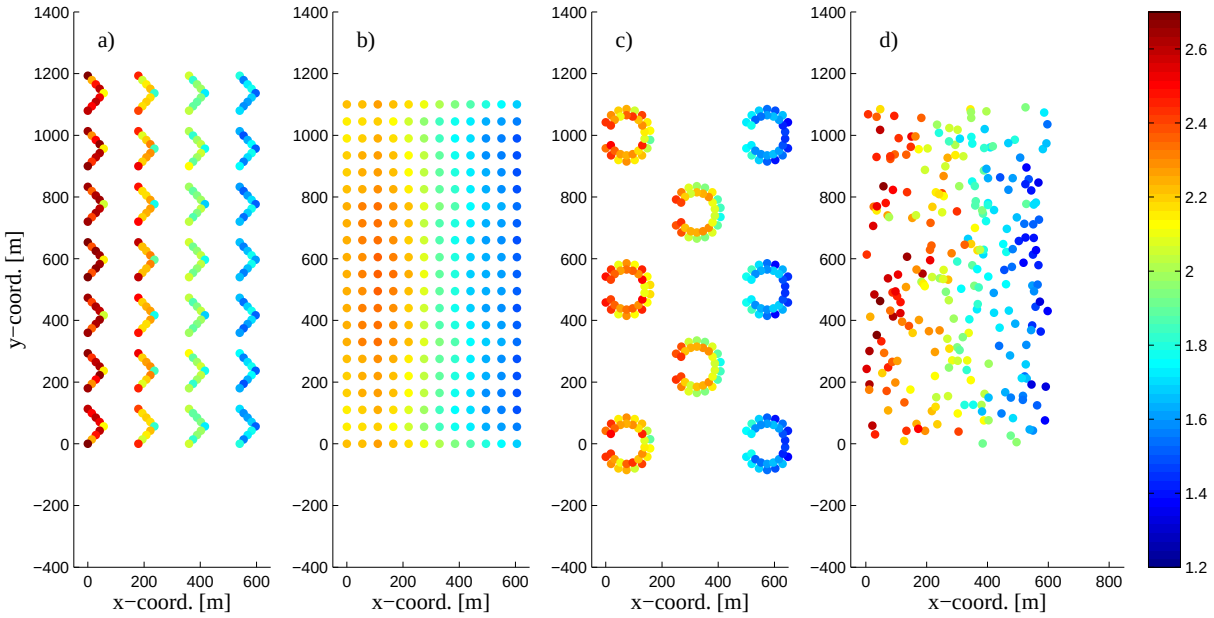

Figure 3: Comparison between the time-averaged power per WEC for four different global geometries. The power scale ranges from 1.2 kW to 2.7 kW per WEC, as depicted by the colorbar. The sea state is categorized by energy period $T_e = 5.47$ s and significant wave height $H_s = 1.02$ m and the incoming wave propagates along the x-axis. The configurations are further compared in figure 4.

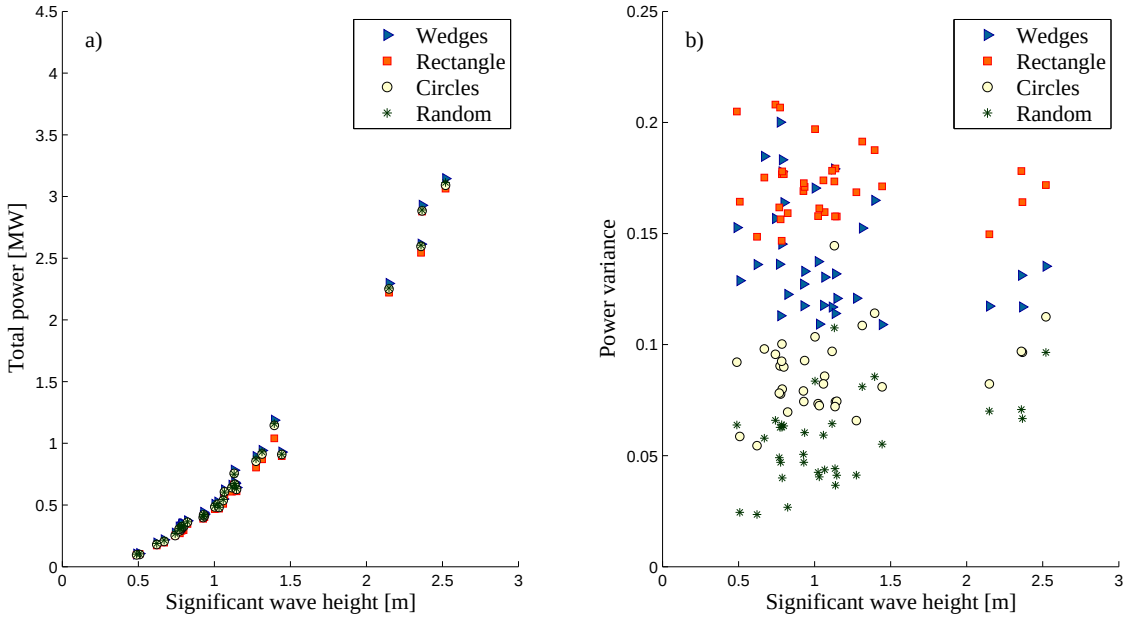

Figure 4: Comparison between the four different global geometries pictured in figure 3. All configurations have comparable energy absorption. However, power variance differs significantly between the four geometries; the rectangular and random geometries provide the worst- and best case scenarios, respectively.

For engineering purposes, in order to compare different park geometries it is of high value to compare the length of sea cable needed, since the cost of sea cable is one of the largest costs associated with the construction of a wave energy park. To get a rough value of the minimum length of sea cable required for the different park configurations, the shortest distance connecting all the WECs has been calculated as a solution to the traveling salesman problem [26]. After approximately 20 000 iterations, the shortest distance connecting all WECs in the four configurations was calculated to 9.5 km for the wedge geometry, 9.9 km for the circular, 13 km for the random geometry and 15 km for the rectangular. Hence, cable length of the wedge and circular geometries are roughly two thirds of the cable length in the randomized and rectangular geometries. In real wave energy parks, all WECs will not be connected to another WEC, but rather to a low voltage substation, from which a cable will be connected to either a medium voltage substation or directly to shore [27, 28]. Nevertheless, the shortest distance between all the WECs presented above gives a hint of the minimum length of sea cable needed. As can be seen, the wedge and the circular configurations are comparable and have the shortest distance between all WECs.

In figure 4, the performance of the four different wave energy parks has been compared for the wide range of sea states listed in table 1. The study is similar to the one performed using the numerical method for smaller parks with 32 WECs in [11]. As can be seen from the figure, the time-averaged total power of the park increases more or less strictly with increasing significant wave height, and the performance of the four geometries is comparable, with the wedge geometry absorbing slightly more power than the other three configurations. However, the power fluctuations vary heavily between the four parks. The mean variance over all sea

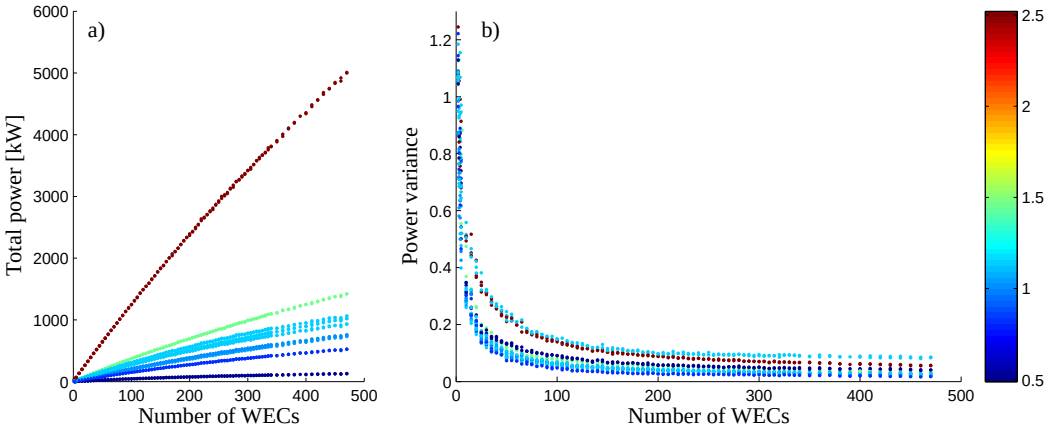

Figure 5: Total power and power variance for wave parks as a function of the number of WECs. The coordinates of the WECs are distributed uniformly random in an area comparable to the area of square parks with WECs on 50 m distance from each other. Each park is computed two times for different random coordinates. In addition, each configuration is studied for nine different sea states, characterized by the significant wave height $H_s \in [0.45, 2.52]$ m, with values shown in the color bar.

states is 0.17 for the rectangle, 0.14 for the wedge geometry, 0.087 for the circular and 0.057 for the random geometry. The lowest variance obtained is 0.024 for one of the sea states and the random geometry. Hence, according to the simulations, the fluctuations in the park with rectangular global geometry are roughly twice of the circular park, and three times larger than for the random geometry.

4.2. Fluctuations as a function of number of WECs

In figure 2, the power and power variance for a wave energy park are studied as functions of the number of WECs in the park, up to $32 \times 32 = 1024$ WECs in the approximate analytical method. The distance between adjacent devices is kept constant to 20 m and only one sea state is used in the simulations.

As expected, both the average power per WEC and the power fluctuations reduce with the number of WECs. According to the simulations with the approximate analytical method, a park with 64 devices has a variance of $v = 0.36$ and average power of 5.2 kW per WEC, whereas a park of the double size has $v = 0.29$ and average power 4.9 kW, and a park with almost ten times as many devices have variance $v = 0.17$ and average power 3.4 kW per WEC.

However, in [12], the variance was found to be a function not only of the number between the buoys, but also to depend strongly on the given sea state and on the separating distance between adjacent devices. To study the variance as a function of the number of devices, but eliminate the dependency of the distance between the buoys and the given sea state, here we have also performed a second parameter study where the number of WECs has been varied. The coordinates of the WECs have been distributed randomly such that a park of N_b WECs occupies an area of $A = 50^2(\sqrt{N_b} - 1)^2$, which would give the same area as for a square park with 50 m distance between adjacent WECs. None of the buoys have been allowed to be in closer proximity to each other than 20 m. To eliminate the factor of the separation distance, two configurations with different random coordinates have been studied for each number of WECs.

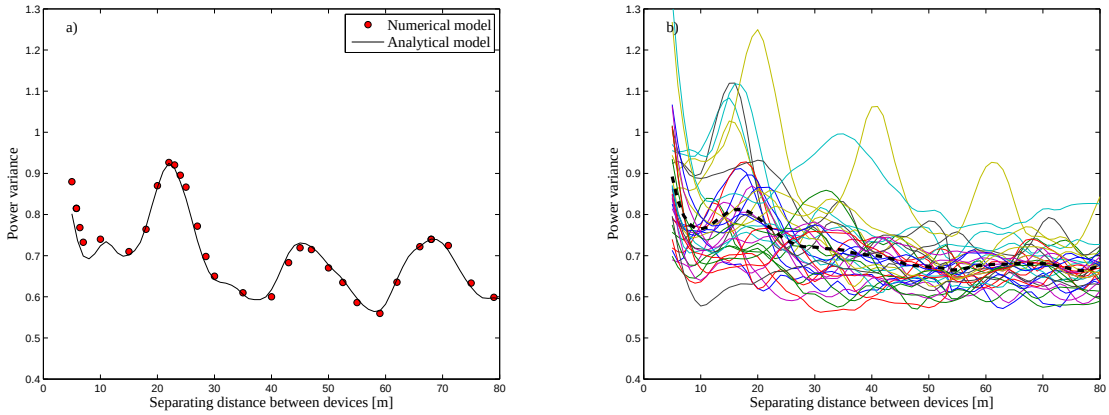

Figure 6: Power variance in a park of 9 WECs in a square lattice as a function of the separating distance between devices. a) Sea state number 35 in table 1 is used in the simulations, both for the numerical and approximate analytical method. The agreement between the methods is good and the fluctuations display a clear oscillatory behavior as a function of the separating distance. b) When taking an average over all sea states 1-34, the oscillatory behaviour is not longer present (thick dotted line). A small peak is obtained at distance $D = 18$ m.

For each configuration, nine different sea states have been used in the simulations to eliminate the dependency of wave climate, namely the sea states number 2, 13, 15, 16, 25, 27, 28, 32 and 33 in table 1. These sea states were chosen since they can be compared pairwise: number 13 and 27 share the same significant wave height, 15 and 16 the same energy period and 25 and 28 roughly the same significant wave height and also since they cover a broad spectrum of significant wave heights. Hence a total of 18 different simulations are run for each number of WECs. The result is plotted in figure 5.

As seen in the figure, the reduction of the power fluctuations with the number of devices follows the same pattern as the simulations for square parks with constant separating distance of 20 m, as plotted in figure 2. The colors in figure 5 display the significant wave height for the sea state used in the simulations. Again, the total power of the park increases strictly with the number of devices, and also with increasing significant wave height. One important difference between the square parks in figure 2 and the random parks in figure 5, is that a low variance is obtained earlier in the random geometry. Hence, increasing the amount of WECs in a random park, say from 50 to 100 WECs, gives less gain in lowered power fluctuations, as would be the case for a square park.

4.3. Power fluctuations as function of separating distance

In [12], the power fluctuations were studied as a function of the separating distance between adjacent devices in a park. An oscillatory behavior was found, but it was also concluded that the behavior was sea state dependent, and that further studies were needed. In [13], the problem was approached again with both the numerical and the approximate analytical method. As seen in figure 6a (also published in [13]), the power variance fluctuates as a function of the separating distance between adjacent units, and the approximate analytical model resembles the results from the numerical method remarkably well. These results motivated further parameter studies using the analytical method.

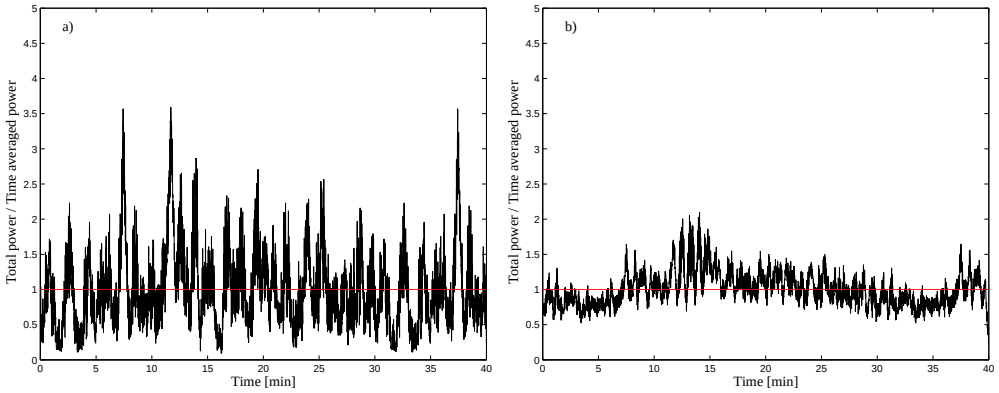

Figure 7: Total power divided by time averaged total power for a park of 32 and 1024 WECs over a time span of 40 minutes. The park configurations are circles with 32 WECs in each; the parks consist of 1 and 32 circles, respectively.

In figure 6b, the power fluctuations in a park of 3×3 WECs in square lattices are studied as a function of the separating distance between devices. The sea states 1-34 in table 1 were used in the simulations. Whereas it is evident that some of the sea states display a clear oscillatory behavior, this appearance vanishes when averaging over all the sea states (thick dotted line). This indicates, that in real wave energy parks where the wave climate is changing over the days, no optimal separating distance can be found that minimizes the power fluctuations.

However, a small peak in figure 6b can be found at separating distance around 18 m. Hence, for the point-absorber WEC studied in this paper and for the most occurring sea states at the test site, separating distances between $15 < D < 20$ m should be avoided to prevent high power fluctuations. For other wave climates and characteristic dimensions of devices, this study would have to be remade to identify any non-optimal separating distances.

4.4. Wave energy parks in the MW range

The four park configurations in figures 3-4 contain roughly 250 WECs and all lie in the MW range, as can be seen in figure 4a. In figure 7, the total power divided by the time averaged power of two wave energy parks has been plotted over a time period of 40 minutes. The first park consists of one double semi-circle with 32 WECs, the second park consists of 32 such circles and has a total of 1024 WECs. The separation distance is roughly 20 m between adjacent devices in the circles. The sea state number 30 in table 1 is used in the simulations, characterized by $T_e = 6.25$ s and $H_s = 2.37$ m.

For the construction of economically viable electrical systems for wave energy parks, it is desirable to reach a ratio close to one between the actual total power and the time averaged total power of the park. From the figure, one can see that the smaller park has power peaks that are 3.5 times higher than the average, whereas the power peaks of larger park are only 2 times higher. The time averaged total power in the small park is 0.4 MW. Multiplying this value with 32 would give an expected total power of 12.8 MW, but the actual total power obtained in the large park is only 8.1 MW, showing the destructive interference between WECs in larger parks. The power variance is 0.28 for the small park and 0.055 for the large park.

5. Summary and conclusions

For the design of economically viable and effective wave energy parks, parameters affecting the power fluctuations and the total output power must be considered carefully. In this paper, we have studied properties of large wave energy parks as functions of some parameters such as the global geometry of the park. Other parameters than the ones discussed here are also relevant for the performance of wave energy parks. Some of these, such as the direction of the incoming wave and the local geometry, were approached in a previous paper [12] and have also been discussed elsewhere, e.g., [7, 29–33]. In this paper, we have restricted the study to include global geometries, number of devices, separating distance between devices, and sea states.

It should be emphasized that a state-of-the-art software such as WAMIT provides a more flexible and accurate method than the approximate analytical method used here. Nevertheless, standard numerical software tend to be very heavy when the number of interacting units in the park grows, and the approximate model provides a way to study very large parks and enables fast parameter studies of arrays. The model includes interaction by radiated waves but neglects scattering between buoys. It has been validated against the numerical method for small parks, where the the numerical method is still efficient. The good agreement between the methods has motivated the use of the approximate model for larger parks. The approximate model can give relevant results and guidelines regarding the design of wave energy parks. However, since the model has not been validated or verified for large arrays, the results should be regarded as qualitative rather than quantitative. From the discussion in section 3.3, the obtained values with the approximate analytical method used in this paper could be expected to provide upper bounds for large parks. Moreover, the method describes only a simplified system of point-absorbers and wave energy parks and for more accurate simulations, more realistic models need to be used. An approach to include multiple scattering effects while keeping the computational cost low by introducing a maximal interaction distance is presented in [34].

In section 4.1, the performance of wave energy parks was studied as a function of the global geometry of the array. Four geometries with roughly 250 WECs were compared: wedges, rectangular, circles and random. The total power was comparable in the four parks and increased with increasing significant wave height. The power fluctuations were largest in the rectangular, roughly 1.2 times higher than the wedge geometry, two times higher than the circular and three times higher than in the random geometry, where the lowest fluctuations were obtained. Taking into account also the roughly estimated cable length required in the parks, the circular geometry is distinguished as the best geometry of the four studied. The same conclusion was reached in [11], where rectangular, semi-circular and randomized small park of 32 WECs were compared using the numerical method where full hydrodynamical interactions are included.

In section 4.2, we studied how increasing the number of WECs in a park affects the power fluctuations and the average power per WEC. As seen in figure 2, placing WECs in arrays is important to lower the fluctuations. However, the gain for adding more WECs to already large parks is small; doubling from 50 to 100 WECs decreases the variance with roughly 21%, but doubling again from 100 to 200 WECs decreases the variance with only 19%, although twice the amount of devices were added. As seen in figure 5, this decrease of power fluctuations is even smaller in wave energy parks with random geometries, since the fluctuations are already quite low for medium sized parks. Since, in realistic situations, the positions of the buoys will not be fixed on exact lattice points, but instead tend to drift off their mean positions, real wave energy parks will always be slightly randomized, and the effect of adding more devices to already large parks is small. As a rule of thumb, the point-absorber WECs should be placed together at least in

small clusters to avoid very large power fluctuations, but other means, such as designing the park geometry appropriately, should be applied to lower the fluctuations further without significantly lowering the total power.

In section 4.3, the power fluctuations were studied as a function of the separating distance between adjacent devices. Whereas some sea states display a clear oscillatory behavior as function of the separating distance, the oscillations look different for different sea states, and is even non-existent for some. When averaging the power variance for a range of 34 common sea states at the west coast of Sweden, the oscillatory behavior disappears. This indicates that it is impossible to find a separating distance between devices that minimizes the power fluctuations for all present sea states. However, as discussed in section 4.3, some separating distances can be found that should be avoided to prevent large fluctuations. In the case studied here, this non-optimal separating distance is between $15 < D < 20$ m.

Section 4.4 treated the total power and the power fluctuations of two parks containing semicircles of 32 devices: a small park consisted on one circle only, and a large park consisted of 32 such circles, to a total of 1024 WECs. Increasing the number of devices 32 times implied that the variance was lowered by 5 times, and that the total power was increased by 20 times. Hence, again the conclusion can be drawn that the gain of increasing the number of devices in already large parks is not very large, due to the already low fluctuations, and to the destructive interference between WECs.

Acknowledgements

This project is supported by StandUp for Energy, Uppsala University, Carl Tryggers Stiftelse, the Swedish Energy Agency, Bengt Ingeströms scholarship fund and the Wallenius foundation.

[1] K. Budal, J. Falnes, A resonant point absorber of ocean-wave power, Nature 256 (1975) 478–479, with Corrigendum in Vol. 257, p. 626.
[2] R. Shaw, Wave Energy - A Design Challenge, Ellis Horwood Ldt, Chichester, UK, 1982.
[3] S. Salter, World progress in wave energy - 1988, The Int. J. of Ambient Energy 10 (1989) 3–24.
[4] K. Thorburn, M. Leijon, Farm size comparison with analytical model of linear generator wave energy converters, Ocean Engineering 34 (5-6) (2007) 908–916.
[5] J. Tissandier, A. Babarit, A. Clement, Study of the smoothing effect on the power production in an array of SEAREV wave energy converters, in: The 18th Int. Offshore and Polar Engineering Conference, Vancouver, Canada, 2008.
[6] J. Sjolte, G. Tjensvoll, M. Molinas, Power collection from wave energy farms, Appl. Sci. 3 (2013) 420–436.
[7] M. Vicente, M. Alves, A. Sarmento, Layout optimization of wave energy point absorbers arrays, in: Proc. of the 10th EWTEC conference, Aalborg, Denmark, 2013.
[8] A. Babarit, On the park effect in arrays of oscillating wave energy converters, Renewable Energy 58 (2013) 68–78.
[9] M. Rahm, O. Svensson, C. Boström, R. Waters, M. Leijon, Experimental results from the operation of aggregated wave energy converters, Renewable Power Generation, IET 6 (3) (2012) 149–160.
[10] V. Stratigaki, P. Troch, T. Stallard, D. Forehand, J. Kofoed, M. Folley, M. Benoit, A. Babarit, J. Kirkegaard, Wave basin experiments with large wave energy converter arrays to study interactions between the converters and effects on other users in the sea and the coastal area, Energies 7 (2) (2014) 701–734.
[11] J. Engström, M. Eriksson, M. Göteman, J. Isberg, M. Leijon, Performance of a large array of point-absorbing direct-driven wave energy converters, J. Appl. Physics 114 (2013) 204502.
[12] M. Göteman, J. Engström, M. Eriksson, J. Isberg, M. Leijon, Methods of reducing power fluctuations in wave energy parks, J. Renewable & Sustainable Energy 6 (2014) 043103.
[13] M. Göteman, J. Engström, M. Eriksson, J. Isberg, M. Leijon, Analytical and numerical approaches to optimizing fluid-structure interactions in wave energy parks, in: Proc. of the International Workshop on Water Waves and Floating Bodies (IWWWFB), Osaka, Japan, 2014.
[14] H. Kagemoto, D. Yue, Interactions among multiple three-dimensional bodies in water waves: an exact algebraic method, J. Fluid Mech. 166 (1986) 189–209.
[15] M. Leijon, R. Waters, M. Rahm, O. Svensson, C. Boström, E. Strömstedt, J. Engström, S. Tyrberg, A. Savin, H. Gravråkmo, H. Bernhoff, J. Sundberg, J. Isberg, O. Ågren, O. Danielsson, M. Eriksson, E. Leijerskog, B. Bolund,

S. Gustafsson, K. Thorburn, Catch the wave to electricity: The conversion of wave motion to electricity using a grid-oriented approach, IEEE Power & Energy Magazine 7 (1) (2009) 50.
[16] R. Krishna, O. Svensson, M. Rahm, S. Kottayil, R. Waters, M. Leijon, Analysis of linear wave power generator model with real sea experimental results, Renewable Power Generation, IET 7 (5) (2013) 574–581.
[17] R. Waters, M. Stålberg, O. Danielsson, O. Svensson, S. Gustafsson, E. Strömstedt, M. Eriksson, J. Sundberg, M. Leijon, Experimental results from sea trials of an offshore wave energy system, Appl. Phys. Lett. 90 (034105).
[18] R. Waters, J. Engström, J. Isberg, M. Leijon, Wave climate off the Swedish west coast, Renewable Energy 34 (6) (2009) 1600–1606.
[19] R. Yeung, Added mass and damping of a vertical cylinder in finite depth waters, Applied Ocean Research 3 (3) (1981) 119–133.
[20] M. Eriksson, R. Waters, O. Svensson, J. .Isberg, M. Leijon, Wave power absorption: Experiments in open sea and simulation, Journal of Applied Physics 102 (084910).
[21] K. Budal, Theory for absorption of wave power by a system of interacting bodies, J. Ship Res 21 (1977) 248.
[22] D. Evans, Some analytic results for two- and three-dimensional wave energy absorbers, Power from Sea Waves, Academic Press, 1980, p. 213.
[23] J. Falnes, Radiation impedance matrix and optimum power absorption for interacting oscillators in surface waves, Appl. Ocean Res. 2 (1980) 75.
[24] S. Mavrakos, P. McIver, Comparison of methods for computing hydrodynamic characteristics of arrays of wave power devices, Applied Ocean Research 19 (5–6) (1997) 283–291.
[25] P. McIver, Some hydrodynamic aspects of arrays of wave energy devices, Applied Ocean Research 19 (1994) 283–291.
[26] J. Kirk, Matlab code for travelling salesman problem - genetic algorithm, MATLAB Central [Online] Available: www.mathworks.com/matlabcentral/fileexchange/13680 (2007).
[27] R. Ekström, M. Leijon, Grid connection of wave power farm using an n-level cascaded h-bridge multilevel inverter, Journal of Electrical and Computer Engineering 2013 (2013) 562548, 9 pages.
[28] M. Rahm, C. Boström, O. Svensson, M. Grabbe, F. Bülow, M. Leijon, Offshore underwater substation for wave energy converter arrays, IET Renewable Power Generation 4 (6) (2010) 602–612.
[29] C. Fitzgerald, G. Thomas, A preliminary study on the optimal formation of an array of wave power devices, in: Proc. of the 7th EWTEC, Porto, Portugal, 2007.
[30] H. Wolgamot, R. E. Taylor, P. Taylor, C. Fitzgerald, The interaction factor for wave power in arrays, in: Proc. of the International Workshop on Water Waves and Floating Bodies (IWWWFB), Athens, Greece, 2011.
[31] J. McNatt, V. Venugopal, D. Forehand, The cylindrical wave field of wave energy converters, in: Proc. of the 10th EWTEC, Aalborg, Denmark, 2013.
[32] Y.-C. Chang, W.-M. Huang, Y.-C. Chow, C.-C. Lind, S.-Y. Tzang, Experimental investigations on two bottom-hinged wave energy converters in tandem operations at different separating distances, in: Proc. of the 10th EWTEC conference, Aalborg, Denmark, 2013.
[33] B. Child, P. L. Weywada, Verification and validation of a wave farm planning tool, in: Proc. of the 10th EWTEC conference, Aalborg, Denmark, 2013.
[34] M. Göteman, J. Engström, M. Eriksson, J. Isberg, Numerical and semi-analytical methods for optimizing wave energy parks, in: Proc. of the International Conference on Hydrodynamics (ICHD) 2014, Singapore, 2014.